Growth substrate induced functional changes elucidated by FTIR and Raman spectroscopy in in-vitro cultured human keratinocytes.

Aidan Meade
Dublin Institute of Technology, aidan.meade@dit.ie

Fiona Lyng
Dublin Institute of Technology, Fiona.lyng@dit.ie

Peter Knief
Dublin Institute of Technology

Hugh Byrne
Dublin Institute of Technology, Hugh.byrne@dit.ie

Follow this and additional works at: http://arrow.dit.ie/radart
Part of the Physics Commons

Recommended Citation

Growth substrate induced functional changes elucidated by FTIR and Raman spectroscopy in in-vitro cultured human keratinocytes

AIDAN D. MEADE [1,2], FIONA M. LYNG [2], PETER KNIEF [3] AND HUGH J. BYRNE [3]

1. School of Physics, Faculty of Science, Dublin Institute of Technology, Kevin Street, Dublin 8, Ireland.

2. Radiation and Environmental Science Centre, Focas Institute, Dublin Institute of Technology, Camden Row, Dublin 8, Ireland.

3. Focas Institute, Dublin Institute of Technology, Camden Row, Dublin 8, Ireland.

Tel.: 00353-1-4024691;

e-mail: aidan.meade@dit.ie

Abstract

Non-invasive measurements of cellular function in *in-vitro* cultured cell lines using vibrational spectroscopy require the use of spectroscopic substrates such as quartz, ZnSe and MirrIR etc. These substrates are generally dissimilar to the original *in-vivo* extracellular environment of a given cell line and are often tolerated poorly by cultured cell lines resulting in morphological and functional changes in the cell. The present study demonstrates various correlations between vibrational spectroscopic analyses and biochemical analyses in the evaluation of the interaction of a normal human epithelial keratinocyte cell line (HaCaT) with MirrIR and quartz substrates coated with fibronectin, laminin and gelatin. The findings of this study suggest that there is a correlation between quantitative measurements of cellular proliferative capacity and viability and peak area ratios in FTIR spectra, with replicated differences in similar areas of the observed Raman spectra. Differences in the physiology of cells were observed between the two spectroscopic substrates coated in fibronectin and laminin, but little differences were observed when the cells were attached to gelatin coated quartz and MirrIR slides. The correlations demonstrate the sensitivity of the spectroscopic techniques to evaluate the physiology of the system. Furthermore the study suggests that gelatin is a suitable coating for use in spectroscopic measurements of cellular function in human keratinocytes, as it provides a material that normalises the effect of substrate attachment on cellular physiology. This effect is likely to be cell-line dependent, and it is recommended that similar evaluations of this effect are performed for those combinations of spectroscopic substrate and cell lines that are to be used in individual experiments.

Keywords: Raman/FTIR Spectroscopy, HaCaT keratinocytes, adhesion effects, spectroscopic substrates

1. Introduction

Vibrational biospectroscopy has advanced considerably in recent years, with attention moving from a focus on measurement of the morphology of cellular and tissue species, to, recently, analyses of the relationship between the biochemical content of biological species and the functionality of such species. At present Fourier Transform Infrared Microspectrosopy (FTIRM) and Confocal Raman Microspectroscopy (CRM) have identified in-situ molecular alterations associated with cell death via apoptosis [1-3] or necrosis [4, 5], or as a result of proliferative changes in cellular activity [6-8] or mitosis [9]. It has also been shown that these modalities can identify molecular changes associated with changes in the phenotype of differentiating embryonic cells [10, 11]. A key characteristic of both CRM and FTIRM is their potential to provide non-invasive information on the total, spatially resolved, molecular composition of the sample, without the need for the introduction of extraneous chemical markers into the cell. It has been established that FTIRM is non-toxic to live cells, even at the increased levels of power utilised in Synchrotron Radiation Fourier Transform Infrared Microspectroscopy (SRFTIRM) [12]. CRM, however, has been shown to result in photo-induced effects when visible excitation wavelengths are utilised [13-15] as compared to when wavelengths in the Near IR and IR are utilised (i.e. 785nm and above) [13] with live cell cultures. No such effects have been observed to date with the use of CRM applied to chemically fixed cellular species, however.

It is known that biomaterial surfaces effect significant responses in the cell, but the underlying molecular mechanisms generating these responses remain poorly understood [16]. Non-invasive spectroscopic measurements of cellular function in *in-vitro* cultured cell lines require substrates such as quartz, ZnSe and MirrIR (Ag/SnO$_2$ coated glass for FTIRM from Kevley Technologies) etc. It has been demonstrated that surfaces and scaffolds for cell culture can induce changes in cellular adhesion and motility [17, 18], in their proliferation and differentiation [16, 19], and in gene expression [20], ultimately influencing the fate of the cell [21]. Much of the interaction of adherent cells with their culture substrates is dependent on the surface chemistry [18, 22] and surface energy [23]. When substrates are coated with biocompatible molecules to effect or enhance cellular proliferation, the conformation of the molecule has also been shown to produce changes in the level of response [19].

In this study vibrational spectroscopy is employed to evaluate the physiology of human keratinocyte cell cultures on MirrIR and quartz, which are coated with biocompatible molecules. The spectroscopic data are correlated with both standard absorbance and fluorescence assays as measures of the viability and proliferative capacity of the cells on these coated substrates. The study thus aims to both demonstrate the efficacy of the spectroscopic techniques to evaluate the physiology of the system, and to evaluate the optimum substrates for cell growth for spectroscopic studies.

2. Methods

2.1 Cell Culture and Sample Preparation

A spontaneously immortalized human epithelial keratinocyte cell line (HaCaT) derived from adult skin was used throughout this work. They are normal, non-tumourigenic and p53 mutated adult keratinocytes. The cells are polygonal, of approximately 20 μm diameter, producing a 'cobblestone' appearance in culture [24]. HaCaT cells were cultured in Dulbecco's MEM: F12 (1:1) medium (Sigma, Dorset, U.K.) containing 10% fetal calf serum (Gibco, Irvine, U.K.) 1% penicillin-streptomycin solution 1000 IU (Gibco, Irvine, U.K.), 2mM L- glutamine (Gibco, Irvine, U.K.) and 1μg/ml hydrocortisone (Sigma, Dorset, U.K.). Cells were maintained in an incubator at 37ºC, with 95% humidity and 5% CO_2. Subculture was routinely performed when cells were 80-100% confluent, using a 1:1 solution of 0.25% trypsin and 1mM versene at 37º C.

The present work was performed to evaluate HaCaT cell adhesion to three substrate coatings, fibronectin, laminin and gelatin. Fibronectin is a large multidomain glycoprotein that is found throughout connective tissue, on the surface of cells and within bodily fluids. It facilitates cell adhesion through binding to integrin receptors on the cell surface, subsequently producing regulation of genetic responses in the cell and influencing cell growth and differentiation [25]. Laminin is also a heterotrimeric glycoprotein [26], which facilitates cell adhesion in a similar manner, though it binds to a different set of cellular integrins. Gelatin is a protein by-product of the thermal denaturation of collagen [27, 28].

HaCaT cells were loaded at a concentration of 1×10^5 cells per substrate onto MirrIR (Kevley Technologies, Inc.) and quartz (UQG Optics Ltd.) substrates both uncoated and coated in fibronectin (1μg/ml solution in PBS; from human plasma), gelatin (2% in dH_2O; type B from bovine skin), and laminin (10μg/ml from Engelbreth-Holm-Swarm murine sarcoma). All coating materials were purchased from Sigma-Aldrich and used without further purification. MirrIR slides were cut into 20 x 25 mm pieces, sterilised in ethanol and dried in a laminar flow hood before coating with the substrate molecules. Both spectroscopic substrates were coated in approximately 300 μl of the coatings.

Spectroscopic substrates were incubated for 24 hours at 4^OC in the gelatin solution, for 4 hours at room temperature in the laminin solution, and for 40 mins at room temperature in the collagen and fibronectin solution. The solutions were aspirated from the fibronectin and laminin coated substrates and washed in PBS before deposition of the cell suspension. The solution was aspirated from the gelatin coated spectroscopic substrates and the cell suspension deposited immediately. Cells were cultured on these growth substrates for 3 days before subsequent spectroscopic and fluorescence/absorbance assays. At 3 days, the cells were fixed in 4% formalin in PBS for Raman and FTIR analysis. They were washed in dH_2O and stored in dH_2O at 4^OC for subsequent Raman analysis and in a dessicator until subsequent FTIR analysis.

The fluorescence and absorbance assays were averaged over two independent experiments (n=2), with 3 and 9 replicates per experiment, respectively. Spectroscopic measurements were taken from one experiment performed in triplicate. Control samples are those in which cells are plated directly onto the uncoated spectroscopic substrate.

2.2 Fluorescence and Absorbance Assays

Parallel cultures were prepared in 6-well plates for spectroscopic assay and investigation of biochemical activity (via measures of proliferative capacity (Alamar Blue fluorescence), lysosomal activity (Neutral Red fluorescence) and protein content (Coomassie Blue absorbance)). Each assay utilised a Tecan Genios microplate reader, with a 5x5 matrix of 25 measurements taken for each well of the 6 well plates to minimize point-to-point variations in fluorescent or absorbance activity. The final fluorescence or absorbance measurement was an average of each of the 25 measurements.

Alamar Blue (AB) is a resazurin dye [29] (dark blue, non-fluorescent) which is reduced to resorufin (pink and highly fluorescent) through a redox reaction, the level of which is indicative of cellular proliferation [29, 30]. Throughout this study, the pink, fluorescent molecule resorufin was excited at 540 nm and the fluorescence read at 595 nm. AB was added to the HaCaT cells in DMEM F-12 (15.6 g/L; Sigma-Aldrich) which did not contain phenol red (as this interferes with the fluorescence of resorufin) and $NaHCO_3$ (1.2 g/L) giving a pH of 6.9 $\pm$ 0.2. Neutral Red (NR; 3-Amino-7-dimethylamino-2-methyl-phenazine hydrochloride) is a supravital fluorescent dye which is weakly cationic and can diffuse across the cellular membrane, accumulating in cellular lysosomes [31-33]. Increases in cell wall permeability and lysosome fragility are associated with the latter stages of cell death, thus the level of accumulation of NR in the cell is indicative of the level of viability in a sample of cells. Neutral Red stock solution was prepared using 0.5 mg of NR dye in 100 ml DMEM-F12 minus phenol red indicator [31-33].

The AB/NR working solution was prepared using 5% AB and 1.25% of the NR stock in DMEM-F12 minus phenol red. A range finding study found that a reasonable incubation time with this solution was 1.5 hours (figure 1), and that no quenching of fluorescence was observed when cells were incubated in a mixture of AB/NR. Samples were therefore incubated with 2.5ml of the AB /NR solution at 37°C for 1.5 hours, at which point the AB fluorescence was measured. Samples were then washed once in 2.5 ml PBS and 2.5 ml of a fixative solution containing 1% glacial acetic acid and 50% ethanol in dH_2O, to lyse the cell

and release the NR dye. Cells were then shaken at 240 rpm for 30 mins and fluorescence was read at 650 nm after excitation at 540 nm [31-33].
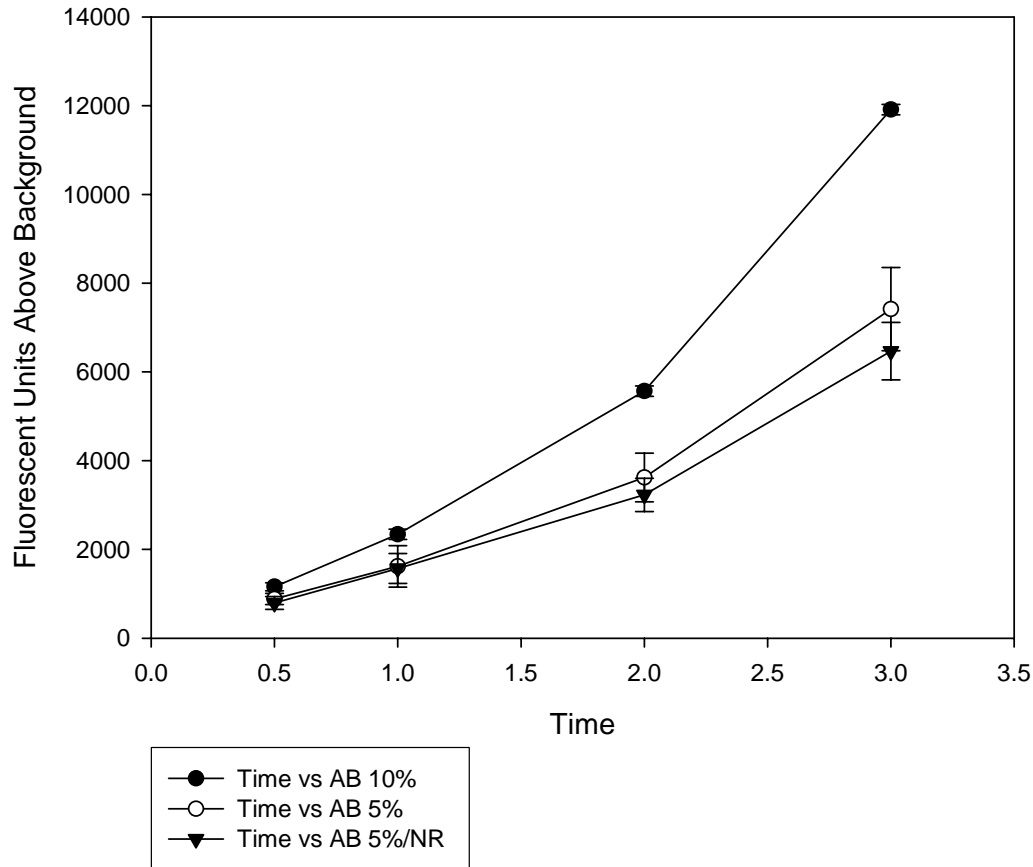

Figure 1. Optimisation of AB Fluorescence Assay

Commassie Blue is a dye which binds to protein within the lysed cell [34]. After binding, and subsequent washing to remove unbound Coomassie Blue, it is possible then to quantify via measurement of absorbance at 595nm (with a reference absorbance measurement at 340nm) the total protein content within the cell [35, 36]. In the present work, after the NR fluorescence had been measured, the samples were washed once in 2.5mls of the fixative solution, 2.5 mls of the Coomassie Blue solution was then added as per Liebsch and Spielmann [35], samples were shaken for 10 mins at 240 rpm and subsequently washed twice in a washing solution (10% ethanol, 5% glacial acetic acid, 85% distilled water), with another shaking step for 10 minutes on the second wash. Finally 2.5 mls of a measuring solution (1M Potassium Acetate in 70% ethanol and 30% distilled water) was added and the samples were shaken in this solution for 10 minutes at 240 rpm. At this point the absorbance of the samples was measured at the wavelengths above.

2.3 Spectroscopic Assays

2.3.1 Raman Spectroscopic Measurements

An Instruments S.A. (Jobin-Yvon) Labram 1B spectrometer was used throughout this work, which is fed by an external Argon-Ion laser operating at 514.5 nm. Throughout the measurements, a x100 objective was employed which gave a spatial resolution of ~1μm at the sample. The system was pre-calibrated to the 520.7 cm^{-1} spectral line of Silicon. The laser power at the objective focus was found to be 15 mW. The Labram system is a confocal spectrometer that contains two interchangeable gratings (600 and 1800 lines/mm respectively). In the following experiments the 1800 lines/mm grating was used, which gave a spectral resolution of around 1 cm^{-1} per pixel. The backscattered Raman signal was integrated for 120 seconds over the spectral ranges from 400 to 1900 and 2500 to 3600 cm^{-1} with respect to the excitation frequency. The detector used was a 16-bit dynamic range CCD detector which is Peltier cooled. Images of the sample were acquired using a video camera within the system.

Spectra were recorded from the cellular nucleus, with 45 spectra recorded per substrate and averaged. A quartz background spectrum was acquired for each individual quartz coverslip used, and subsequently subtracted before averaging. A simple baseline subtraction was performed in Matlab. A Savitsky-Golay filter (5th order, 17 points) was used to smooth spectra. Band assignments were based on the data in table 1, which is taken from numerous publications and reviews [37-41].

Wavenumber (cm^{-1})	Assignment
3070	Amide B (CNH bend)
2960	CH$_3$ stretch (antisymmetric) due to methyl terminal of membrane phospholipids
2936	CH$_3$ stretch
2928	CH$_2$ antisymmetric stretch of Methylene group of membrane phospholipids
2886	CH$_2$ stretch (symmetric) due to methylene groups of membrane phospholipids
2854	CH$_2$ stretch
2739	CH stretch
1736	C=O stretch
1667; 1640	Amide I (protein) C=O stretching of amide coupled to NH$_2$ in-plane bending
1657, 1659	C=C stretch (lipids), Amide I (α-helix, protein)
1611	Tyr (aromatics)
1566	Phe, Trp (phenyl, aromatics)
1550	Amide II absorption due to N-H bending coupled to a C-N stretch
1509	C=C stretch (aromatics)
1452	CH$_2$ stretch deformation of methylene group (lipids)
1439	CH$_2$ def.
1420	CH$_3$ asymmetric stretch (lipids, aromatics)
1397	CH$_3$ bending due to methyl bond in the membrane
1382	COO$^-$ symmetric stretch
1367	CH$_3$ symmetric stretch
1336	Adenine, Phenylalanine, CH deformation
1304	Lipids CH$_2$ twist, protein amide III band, adenine, cytosine
1267	Amide III (α-helix, protein)
1250	Amide III (β-sheet, protein)
1235	Antisymmetric phosphate stretching
1206	C-C stretch, C-H bend
1165	C-O stretch, COH bend
1130	C-C asymmetric stretch
1100, 1094, 1081	PO$_2^-$ symmetric stretch (nucleic acids)
1065	Chain C-C
1056	RNA ribose C-O vibration
1003	Phenylalanine (ring-breathing)
967	C-C and C-N stretch PO$_3^{2-}$ stretch (DNA)
957	CH$_3$ deformation (lipid, protein)
936	C-C residue α-helix
921	C-C stretch proline
898	C-C stretch residue
870	C-DNA
853	Ring breathing Tyr – C-C stretch proline
828, 833	Out of plane breathing Tyr; PO$_2^-$ asymmetric stretch DNA (B-form)
807	A-DNA
786	DNA – RNA (PO$_2^-$) symmetric stretching
746	Thymine
727	Adenine

Table 1. Peak assignments derived from Krishna et al [37], Nijssen et al [38], Synytsya et al [39], Edwards and Carter [40], and Puppels et al [41] (and references therein)

2.3.2 FTIR Spectroscopic Measurements

FTIRM was performed using a Perkin Elmer GX-II spectrometer. The system is equipped with a Mid-infrared source with mid-infrared and far-infrared beam splitters that allow spectroscopic measurements of wavenumber shifts in the range 7000 to 50cm^{-1} with a maximum resolution of 0.3 cm^{-1}. The system is also equipped with a microscope attachment containing a x 40 objective, and is configured with the AutoIMAGE microscope system that

can operate in transmission or reflectance modes. All microscope operations including adjustments to aperture, focus and illumination are fully automated and controlled from an attached PC. The system includes a built-in 35W tungsten halogen illuminator, a motorised stage and a CCD video camera. The FTIRM measurements reported here utilised aperture sizes of 100 x 100 μm, spectral resolution of 4 cm^{-1}, with 64 scans per spectrum. All spectra were acquired in reflection mode, effectively a double transmission after reflection from the broadband MirrIR substrate, with 250 spectra recorded from each sample. The final baseline corrected spectrum from each sample was an average of each of these measurements. IR band assignments as shown in table 2 were employed throughout the study.

Wavenumber (cm^{-1})	Assignment
3328	Amide A (ν -N-H), proteins
3129	Amide B (ν -N-H), proteins
3015	ν =C-H, lipids
2960	ν as -CH$_3$, lipids proteins
2920	ν as -CH$_3$, lipids proteins
2875	ν s -CH$_3$, lipids proteins
2850	ν s –CH$_2$, lipids proteins
1720-1745	ν –C=O, lipids (esters)
1710-1716	ν as –C=O, RNA (esters)
1705-1690	ν as –C=O, RNA, DNA
1654	Amide I ν -C=O (80%), ν - C-N (10%), δ -N-H (10%), α-helix
1630-1640	Amide I ν -C=O (80%), ν - C-N (10%), δ -N-H (10%), β-structure
1610, 1578	ν -C4-C5, ν -C=N, imidazole ring, DNA, RNA
1515	Aromatic tyrosine ring (Lasch et al)
1540-1550	Amide II δ -N-H (60%), ν - C-N (40%), α-helix
1530	Amide II δ -N-H (60%), ν - C-N (40%), β-structure
1467	δ –CH$_2$ lipids, proteins
1455	δ as –CH$_3$ / -CH$_2$ scissoring lipids, proteins
1370-1400	ν -COO$^-$, δ s –CH$_3$ lipids, proteins
1330-1200	Amide III, proteins
1230-1244	ν as –PO$_2^-$, RNA, DNA
1160, 1120	ν -C-O, RNA ribose
1170, 1070	ν as, ν s –CO-O-C, lipids
1090-1084	ν s –PO$_2^-$, RNA, DNA
1060, 1050	ν –C-O, deoxyribose/ribose DNA, RNA
996	RNA stretch and bend ring of uracyl
965	symmetric PO$_4^-$ stretch (DNA) and deoxyribose-phosphate skeletal motions

Table 2. IR Peak assignments (for cellular spectra) derived from Gault et al, [42-44] and Zellmer et al [45] (and references therein).

3. Results and Discussion

3.1 Fluorescence/Absorbance Assays

The results of fluorescence and absorbance measurements of cellular proliferation, viability and total protein content are presented in figures 2-4. All measurements have been normalised to the MirrIR control. Error bars depict the variability at one standard error on the mean of the measurements.
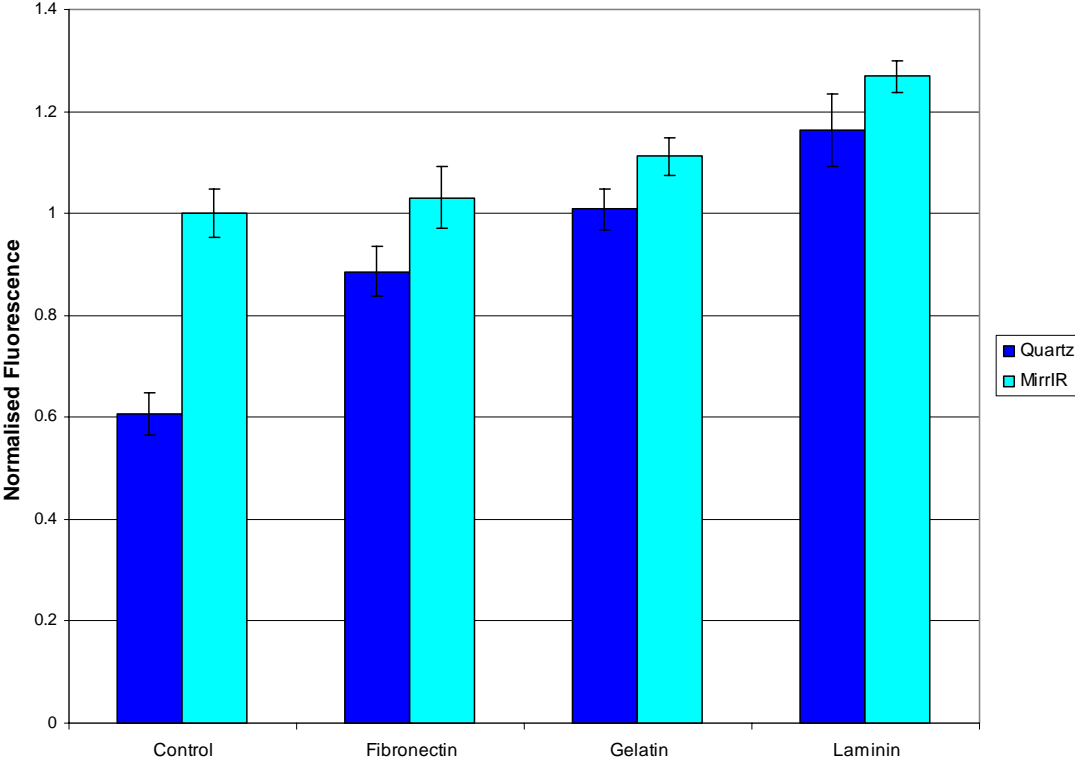

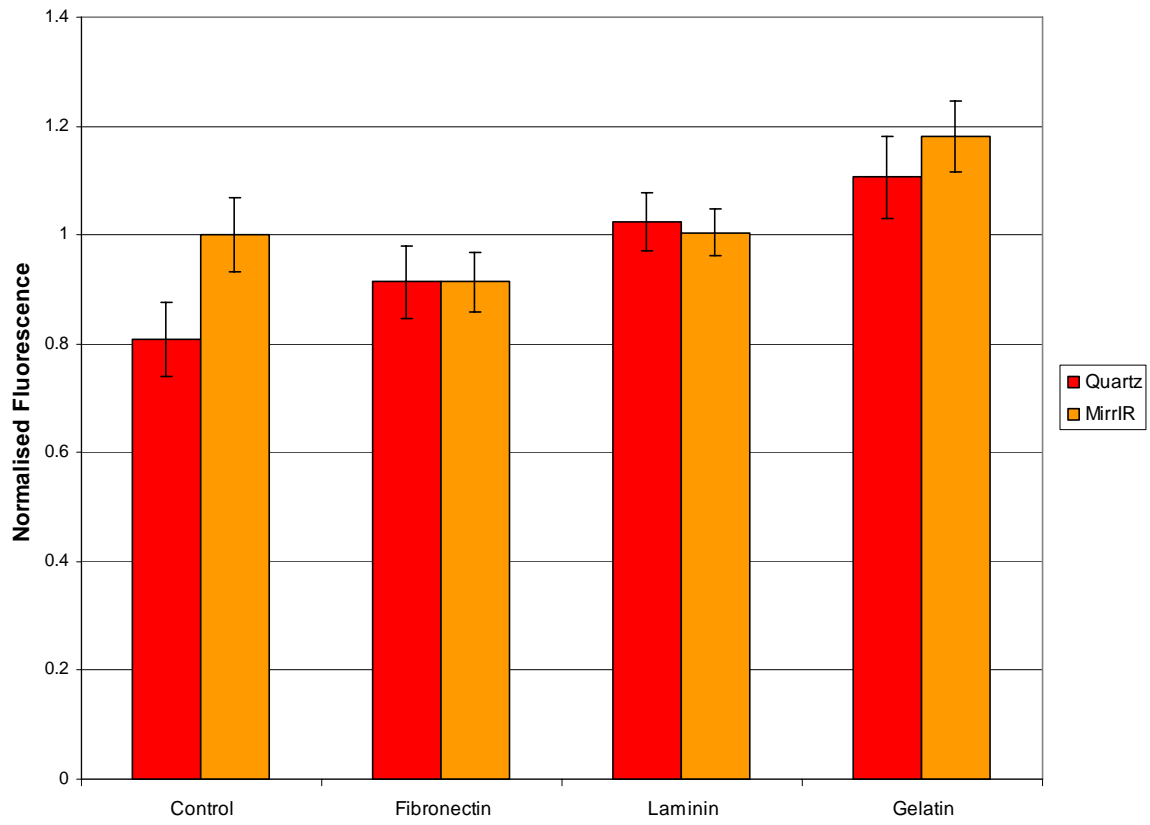Figure 2. Alamar Blue Fluorescence by substrate (Normalised to MirrIR Control for both MirrIR Substrate and Quartz Substrate) .

Figure 3. Neutral Red Fluorescence by substrate (Normalised to MirrIR Control for both MirrIR Substrate and Quartz Substrate).
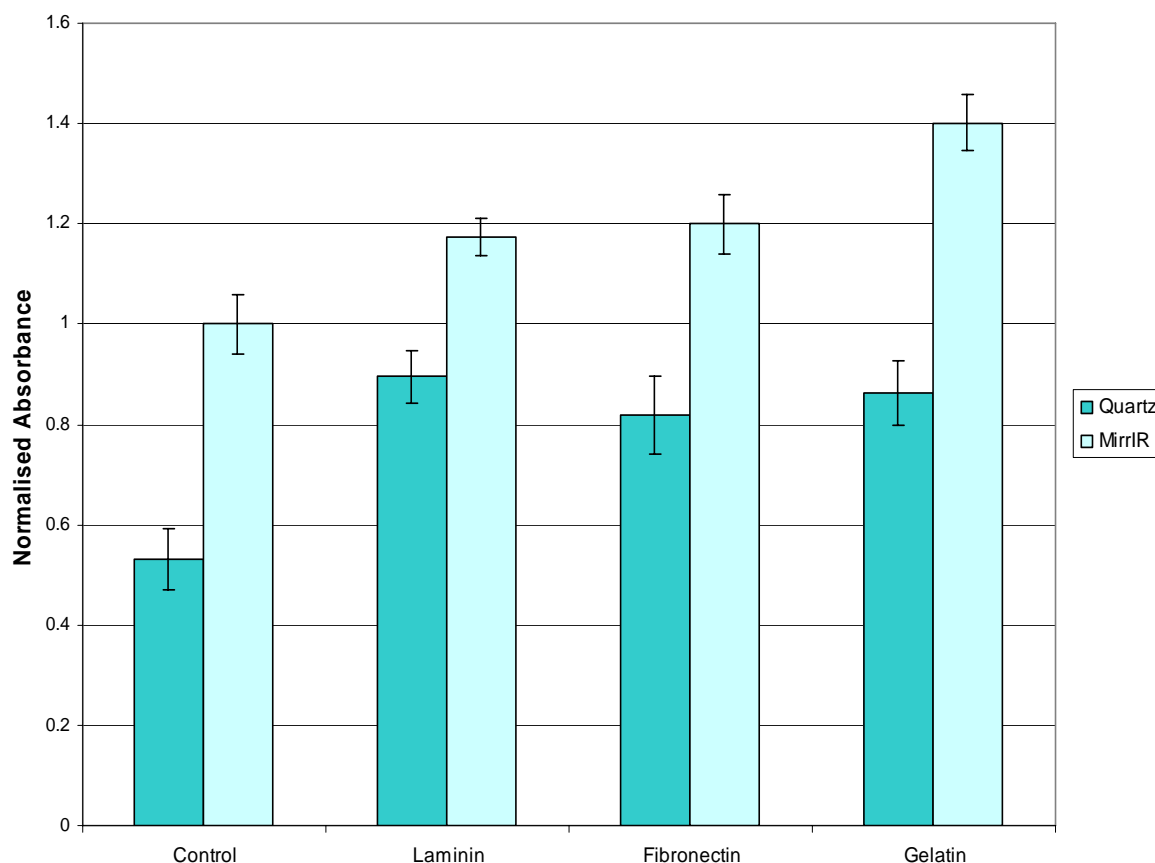
Figure 4. Coomassie Blue Absorbance by substrate (Normalised to MirrIR Control for both MirrIR Substrate and Quartz Substrate).

The general trend in the fluorescence measurements indicates that cellular proliferation, viability and protein content are enhanced by growth of HaCaT keratinocytes on gelatin, fibronectin and laminin. It appears that uncoated quartz induces a marked decrease in cellular proliferation and protein content. The enhancement in proliferation and viability is more pronounced when cells are grown on coated quartz substrates than MirrIR substrates, demonstrating that molecular conformation plays a role in cellular physiology post attachment as shown previously [19]. This also indicates that the Ag/SnO_2 coating on the reflective surface of MirrIR substrates plays some role in promotion of cellular attachment, which may be as a result of surface roughness on the nanometer scale [46-48].

The adhesion of cells to the extracellular matrix (ECM) is mediated by integrin binding [25]. Integrins are cell surface receptor proteins which bind the ECM to the cytoskeletal proteins within the cell, which subsequently stimulates the production and regulation of signalling proteins, such as protein kinase C and EGF [49, 50]. This ultimately results in increasing

proliferation and motility, which is also dependent on the charge distribution presented by the ECM coating molecule to the adhering cell [18-23, 25]. Ultimately the reaction of the cell to such influences are complex, being the cumulative effect of the increased or decreased regulation of a number of stimulatory pathways in the cell, with the end physiological change in any given cell being dependent on the cell and substrate ECM [50, 51]. It has been shown that adhesion of epithelial keratinocytes to fibronectin, collagen I and laminin promotes the activation of EGFR, although this effect can be sustained for various periods of time depending on the ECM molecule [50]. Bearing in mind that this effect is augmented by the conformation of the ECM molecule and its surface charge distribution, it is possible to suggest that the results of the present work (figure 2) indicate increased sustained production of signalling proteins resulting in increased proliferation of keratinocytes cultured on fibronectin, laminin and gelatin coated quartz slides, but only MirrIR slides coated with laminin produce significant changes in keratinocyte proliferation relative to the control. Figure 3 suggests that significant increases in cellular viability, relative to the control, are observed in keratinocytes grown on quartz coated with laminin and gelatin, but only significant increases in viability are observed when keratinocytes are grown on gelatin coated MirrIR slides. Taken together, both these results suggest that a coating such as gelatin provides an ECM that maintains similar proliferation effects on both quartz and MirrIR substrates, while increasing viability, which may be desirable for long-term cultures. Increases in protein content (which are seen as the result of increases in proliferation [6,8 and references therein]) shown in figure 4 may be normalised for spectroscopic purposes by normalising spectra to the Amide I band and/or the CH peak at 2939 cm^{-1} (in the case of Raman spectra) and 3328 cm^{-1} (in the case of FTIR spectra).

Although the measurements here concentrate on one adherent cell line (HaCaT keratinocyte), the adherent effects likely to occur in other cell lines can be speculated from existing research. It is known that the chemistry of the substrate modifies integrin receptor binding and through this cellular proliferation, viability and motility. Doornaert et al [52] have examined the effect of collagen, fibronectin and laminin on human bronchial epithelial cell (HBE) proliferation where similar relationships between substrates have been found as have been observed in the present work. Keselowsky et al [16] have observed hydroxyapatite formation in MC3T3-E1 osteoblasts on fibronectin coated self-assembled monolayers of alkanethiols with CH$_3$, OH, COOH and NH$_2$ terminals, using FTIR spectroscopy. They have found that surface chemistry can affect integrin binding of the cell to the substrate even when utilising the same coating

14

molecule. Sutherland et al [53] have also analysed proliferative effects in human keratinocytes, melanocytes, fibroblasts and myofibroblasts adherent to fibronectin, laminin, collagen and vitronectin with similar results to our work.

3.2 Spectroscopic Assays

Figures 5 and 6 display the results of FTIRM and CRM measurements of HaCaT cells attached to gelatin coated substrates, spectra of the gelatin itself, and spectra of the coated substrate. Note that, as described previously, substrates for cell adhesion are coated by incubation with the solution of coating molecule for a period of time, and are then subsequently washed a number of times in PBS to remove the unbound molecule, as this can subsequently influence the cell behaviour by its presence in the extra-cellular medium. Gelatin has spectral features similar to the HaCaT cells because of its protein nature, but at the thicknesses employed here, these features are not visible. Similar results were observed in spectroscopic measurements of fibronectin and laminin coated substrates [54].

Gazi et al [55] have recently demonstrated that formalin fixation preserves most effectively the subcellular structure within the cell observed by SRFTIR spectroscopy, while O Faolain et al [56] have shown that shifts of up to 10 cm^{-1} are observable in FTIR spectra of formalin-fixed versus fresh tissue, with reduction in the intensity of the C=O band at 1398 cm^{-1}. Other features associated with the presence of formalin within the Raman spectrum occur at 1041 cm^{-1} and 1492 cm^{-1} and can indicate formalin contamination of the sample [57], while fixation has been observed to produce peaks at 1490 cm^{-1} and to reduce the Amide I peak at 1637 cm^{-1} [56]. These features may occur as a result of protein unravelling or amide cross-linking induced by formalin fixation. No such features were observed in either our FTIR or Raman spectra indicating no formalin contamination in the cellular samples. However, the effect of formalin on the protein Amide regions of the spectra, due to formalin-induced amide cross-linking [57], has not yet been investigated in cellular species.

The FTIR spectral features of the HaCaT cells display strong Amide A and Amide B vibrations in the high wavenumber regions (~ 3328 and 3129 cm^{-1} respectively) with strong phospholipid terminal -CH_3 stretching vibrations (both symmetric in the region of 2875 cm^{-1} and antisymmetric in the region of 2960 cm^{-1}) also visible. The Raman spectral features in this region are also dominated by -CH_3 and -CH_2 stretching modes (between 2900 and 2983 cm^{-1}), with a weak Amide A vibration (in the region of 3070 cm^{-1}) and -CH stretch (in the region of 2729 cm^{-1}), and water contributions above 3070 cm^{-1}. Moving to the fingerprint region, the FTIR spectra are strong in the Amide I (peaking at 1654 cm^{-1}) Amide II (peaking

at 1555 cm^{-1}) and Amide III (region from at 1330 to 1200 cm^{-1}) with lipid δ-CH$_2$ and δ-CH$_3$ contributions (in the region from 1467 to 1455 cm^{-1}) and –COO$^-$ stretching vibrations (in the region from 1370 to 1400 cm^{-1}). These bands overlap to some extent in the lower wavenumber region with the –PO$_2^-$ stretching vibration (1090-1084 cm^{-1};1230-1244 cm^{-1}), the C-O stretching vibration of RNA ribose (1160; 1120; 1060; 1050 cm^{-1}), and the symmetric and anstisymmetric stretch of –CO-O-C (lipid, ~1170 and ~1120 cm^{-1}).

Raman spectra of HaCaT cells again display strong Amide I (~1681 cm^{-1}), Adenine/Guanine in plane ring modes superimposed on CH/CH$_2$ vibrations (~1457 cm^{-1}) and Amide III vibrations (~1230-1260 cm^{-1}). Lipid contributions from -CH$_2$ and –CH$_3$ stretching (1308-1398 cm^{-1}) are strong, as are those from –PO$_2^-$ residues of DNA/RNA (1056-1111, 863-935 cm^{-1} and 783-847 cm^{-1}) and Phenylalanine ring breathing modes (1003 cm^{-1}).
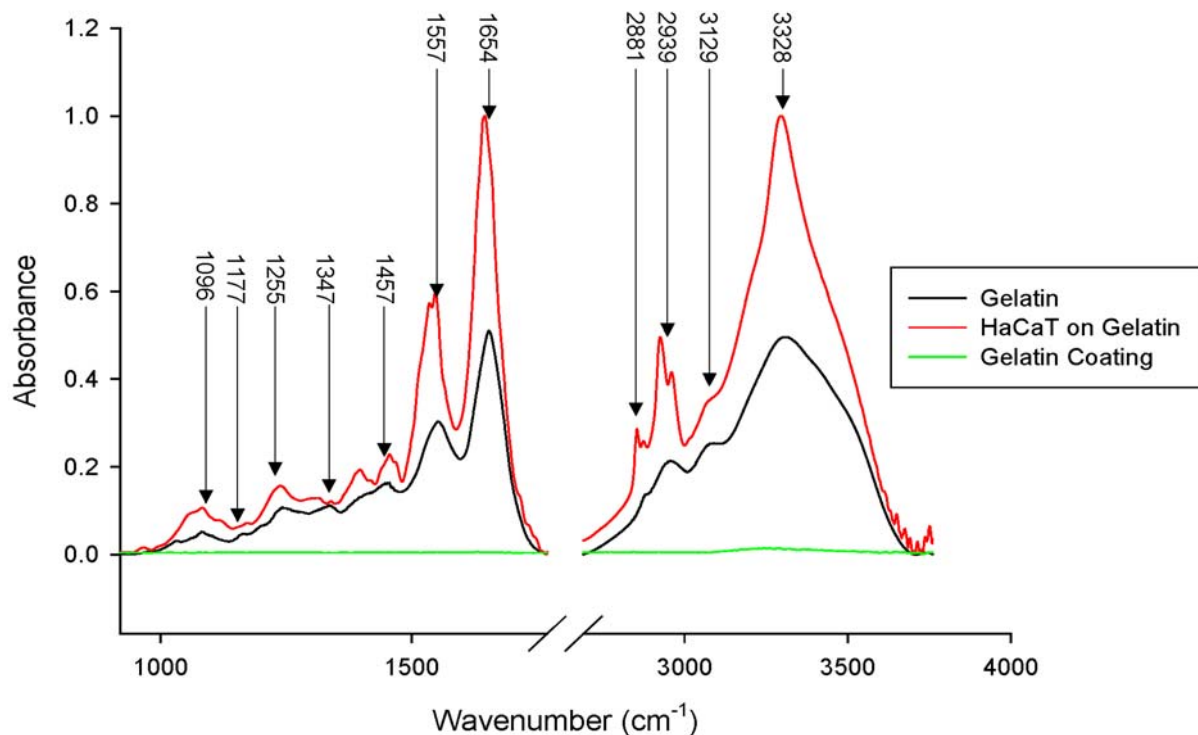

Figure 5. FTIR spectra of gelatin coated MirrIR slide with measured FTIR spectrum of gelatin and that of HaCaT cells grown on gelatin.
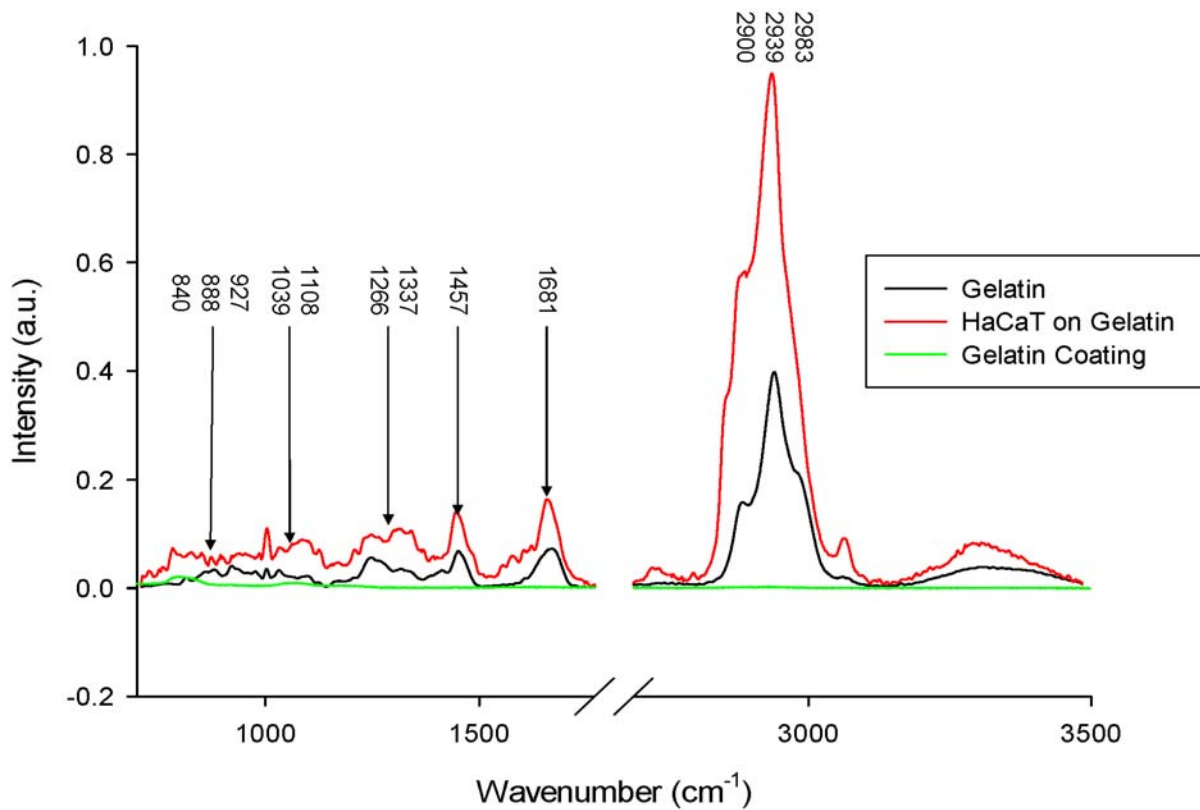
Figure 6. Raman spectra of gelatin coated quartz slide with measured Raman spectrum of gelatin and that of HaCaT cells grown on gelatin.

Results of spectroscopic measurements (in the fingerprint region) of HaCaT cells on coated spectroscopic substrates are shown in figures 7-9(b). Raman spectra were normalised to the CH band intensity at 2939 cm^{-1} (not shown). FTIR spectra are averages of 250 measurements, with normalisation to the Amide I band absorbance at 1654 cm^{-1}.
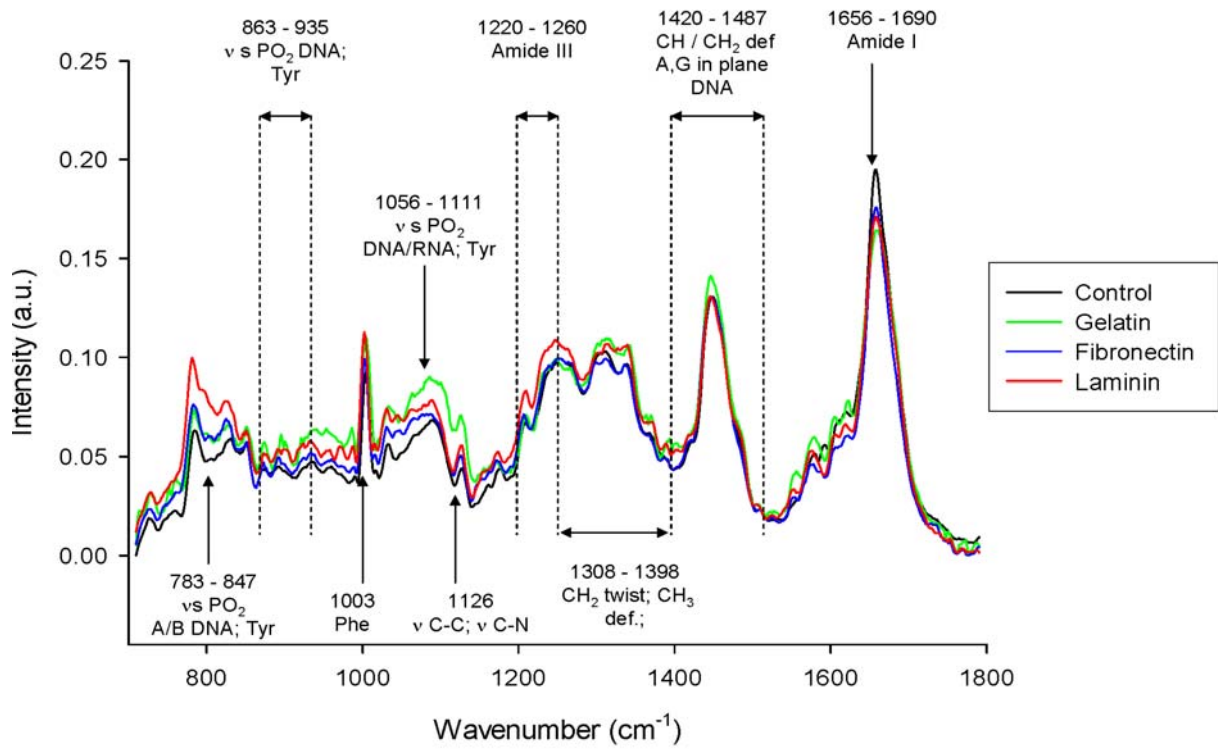
Figure 7. Raman spectra of HaCaT cells on coated spectroscopic substrates in the fingerprint region (700 to 1800 cm⁻¹).
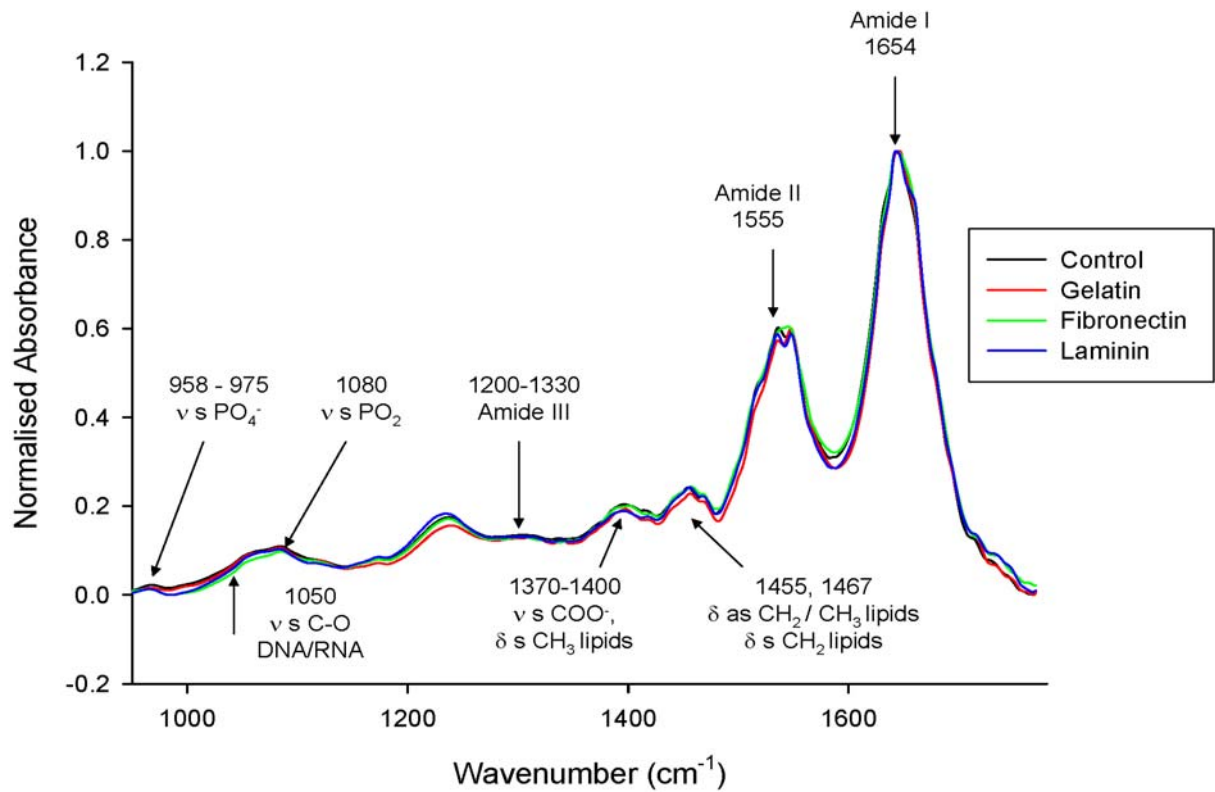

Figure 8. FTIR spectra of HaCaT cells on coated spectroscopic substrates in the fingerprint region (920 to 1770 cm⁻¹).
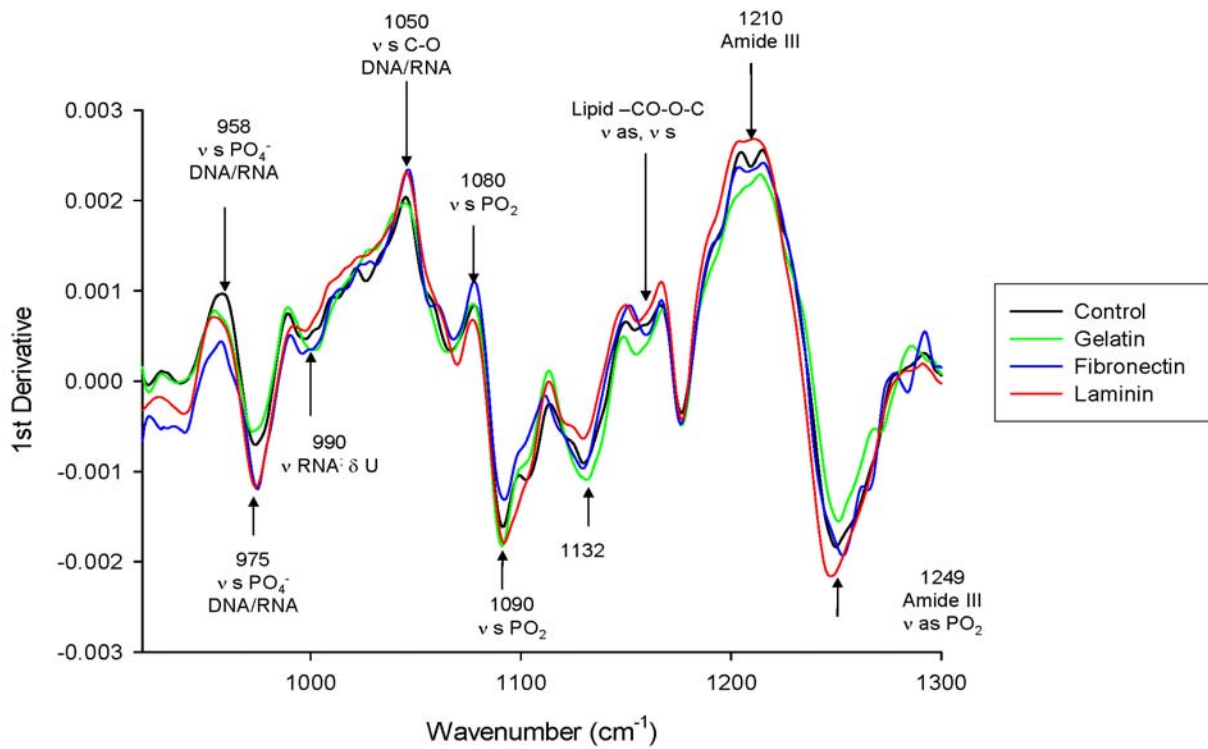
Figure 9(a). First Derivative FTIR spectra of HaCaT cells on coated spectroscopic substrates in the fingerprint region (920-1300 cm^{-1})
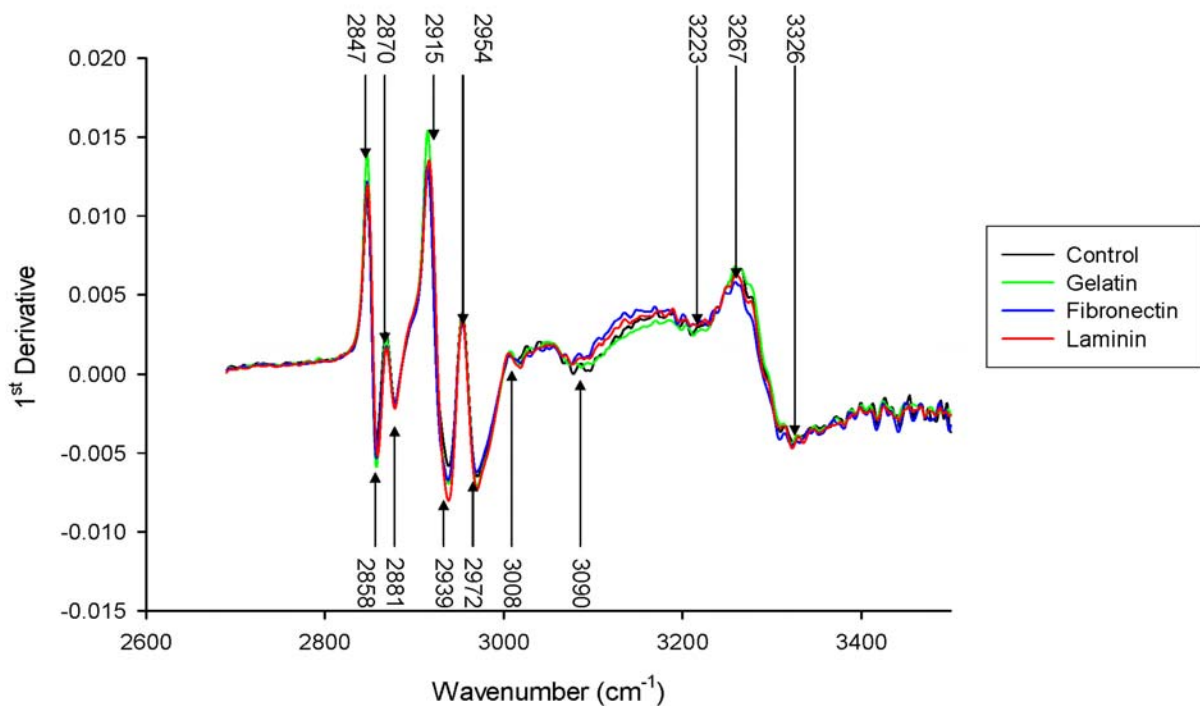

Figure 9(b). First Derivative FTIR spectra of HaCaT cells on coated spectroscopic substrates in the CH region (2690-3500 cm^{-1}).

The first derivative FTIR spectra exhibit shape changes in the HaCaT cell spectra in regions of the spectrum associated with nucleic acid, lipid and protein expression (respectively from 950 to 1090 cm^{-1}, at 1070 and 1170 cm^{-1}, and from 1200-1330 cm^{-1}, with other changes in the lipid and protein regions from 1370-1467 cm^{-1}). Such spectral changes have been seen recently in proliferating mammalian cells [6, 8]. The correlation between cell viability (NR fluorescence) and FTIR spectral changes in the HaCaT cells attached to different substrates was investigated using calculations of band integral ratios from the raw spectra. This correlation is depicted in figure 10 for FTIR spectral measurements (where in this, and all subsequent, plots of band integral ratios, a straight line is overlaid as a guide for the eye to the inferred correlation). The integral of absorbance between 2850 and 3015 cm^{-1} has been taken as an estimate of the total lipid –CH, –CH_2 and –CH_3 bond vibration content (in the CH region, termed 'Lipid CH' here), while the integral of absorbance between 3129 and 3328cm^{-1} has been taken as an estimate of the total protein Amide A and B vibration content (also in the CH region, termed 'Amide AB' here), and the sum of the integrals of absorbance between 1084 and 1090 cm^{-1} and between 1230 and 1240 cm^{-1} have been taken as an estimate of total –PO_2^- bond vibration content. There are some slight contributions from water in the IR spectra in the 3000-3500 cm^{-1} region, evident in figure 9(b), although these should be removed in the peak area ratio of Amide AB to Lipid CH. A correlation between both the ratio of lipid to PO_2^- band areas and the ratio of lipid to Amide A and B band integrals was observed. This may signify that the integrity of lipid, protein, and nucleic acid backbone are crucial to cell viability.

It has been found by Mourant et al [8], by means of fitting base sets to cellular FTIR spectra, that the ratio of RNA to lipid content and the ratio of protein to lipid content increase with increasing cellular proliferation. In the present study, RNA content was estimated using the integral of absorbance from 1710-1716 cm^{-1} (symmetric stretch of C=O in RNA). Lipid content was estimated using an integral of the absorbance from 1370 to 1400 cm^{-1} (COO$^-$ stretch and –CH_3 symmetric bending in protein and lipids), and Amide I, Amide II and Amide III cumulative contributions were estimated using the integral of absorbance from 1630-1654 cm^{-1}, 1530-1550 cm^{-1} and 1200-1330 cm^{-1} respectively. 'Total Protein' was computed using a summation of the Amide I, II and III band integrals. These integrals were compared to quantitative estimates of cellular proliferative capacity from normalised AB fluorescence and are depicted in figure 11. The ratios for each of the absorbance integrals increase with increasing cellular proliferation as found by Mourant et al [8], with the most significant

association between proliferation and the total protein to lipid content. Linear fits have been applied to each set of data as a means of examining the relative degree of association between each of the metrics and cellular proliferation, although in the case of both the Amide I to lipid ratio and the RNA to lipid ratio, this is better served by a 2nd order polynomial fit. It is difficult to ascertain ratios indicative of RNA synthesis (both in FTIR and Raman spectra) because there are so many overlapping bands in this region of the spectrum. This may account for the large error bars seen in the spectral area ratios of RNA vs lipid.

Raman spectral changes are also observable in those parts of the fingerprint region associated with DNA and RNA PO_2^- (862-915 cm^{-1}; 1056-1100 cm^{-1}; 1212-1266), protein (Amide I, 1657-1690 cm^{-1}; Amide III, 1212-1266) and lipid (1397-1452 cm^{-1}). Increases in the regions associated with DNA and RNA, and protein, with decreases in those regions associated with lipid, were observed in cells with increased proliferation (figure 7), which have been noted previously [8]. Quantification of the correlation between the spectra and fluorescence measurements are shown in figures 12 and 13. It should be noted that the control points in each graph in each figure will overlap at 1, and that the SE bars in the direction of each of the peak area integrals is not shown (although these are in all cases less than 5% in either direction). The lipid (estimated from the integral from 2870 to 2975 cm^{-1}) to Amide AB (estimated from the integral from 3048 to 3087 cm^{-1}) and $-PO_2^-$ (estimated from the integral of intensity from 862-915 cm^{-1}) to Lipid band integral ratios (1396-1452 cm^{-1}) were found to increase with increasing NR fluorescence (cell viability), as demonstrated in figure 12. A correlation was also observed between the total protein (estimated via the summation of the area of the Amide I and Amide III band integrals) to lipid ratio, the $-PO_2^-$ to Amide I ratio, the $-PO_2^-$ (due to RNA and estimated from the integral from 783 to 848 cm^{-1}) to lipid (1397-1452 cm^{-1}) ratio and the cellular proliferation as measured by AB fluorescence (figure 13). Similar trends have been observed previously by Short et al [6], where increases in protein and decreases in lipid were observed in proliferating cells, with decreases in RNA and increases in DNA between plateau and exponential phase cells. It is difficult to elucidate spectral changes associated with proliferative effects from Raman spectra, using peak area ratios, due to the large degree of spectral overlap between subcomponents (nucleic acid, protein, lipid etc.) within the spectrum [8]. This difficulty may be lessened through careful choice of spectral intervals for integration, as was the approach adopted here. The spectral changes observed here are consistent with those previously observed in experiments utilising spectral decomposition [8], and as such support the approach adopted here.
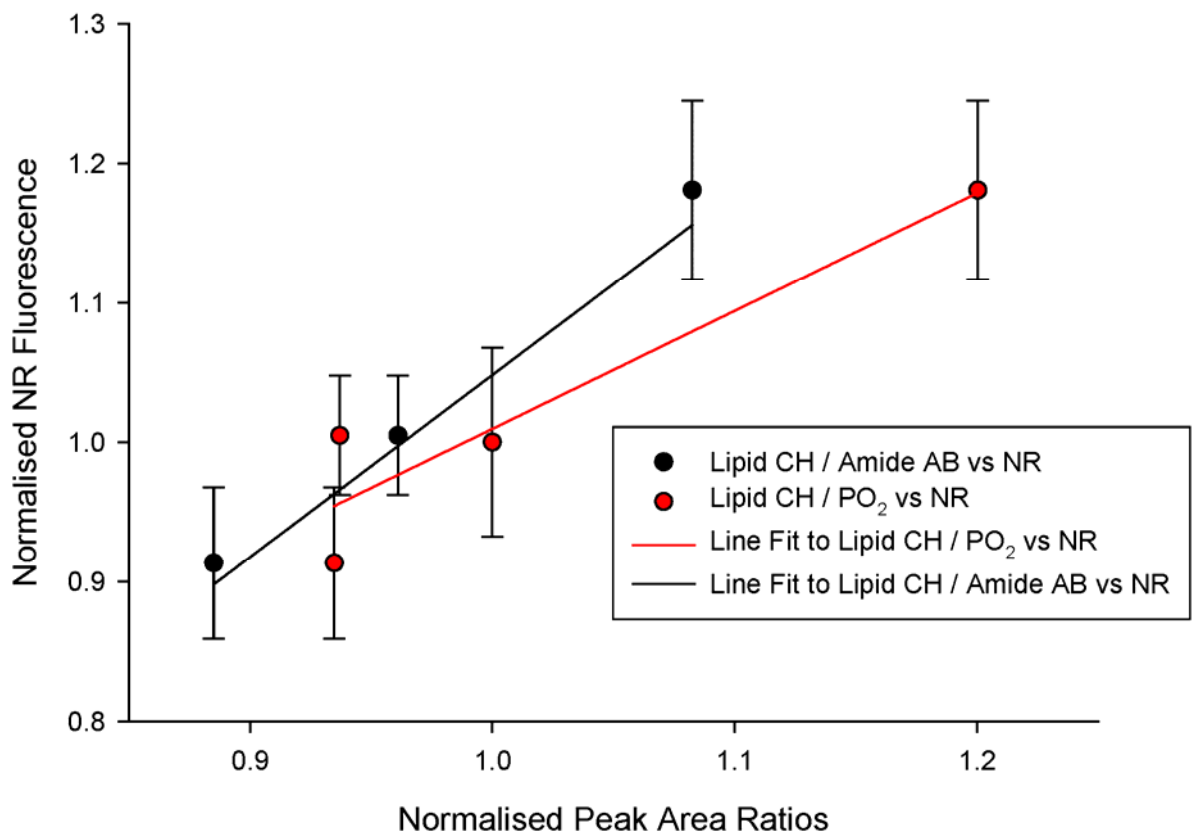
Figure 10.Correlation of various FTIR band integrals (as described in the text) to NR fluorescence (cell viability). All measurements are normalised to the corresponding control measurement.
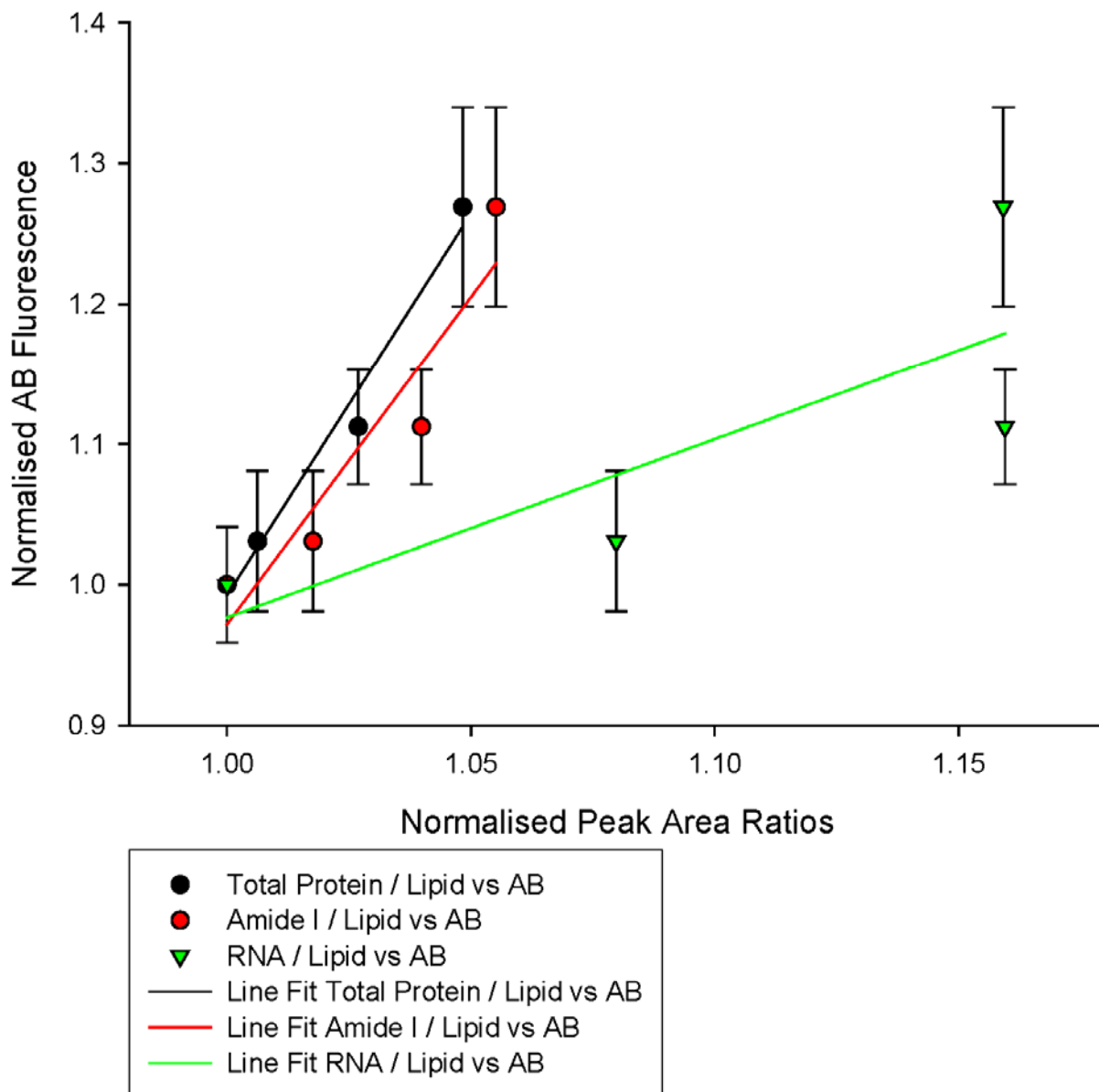
Figure 11. Correlation of various FTIR band integrals (as described in the text) to AB fluorescence (proliferative capacity). All measurements are normalised to the corresponding control measurement.
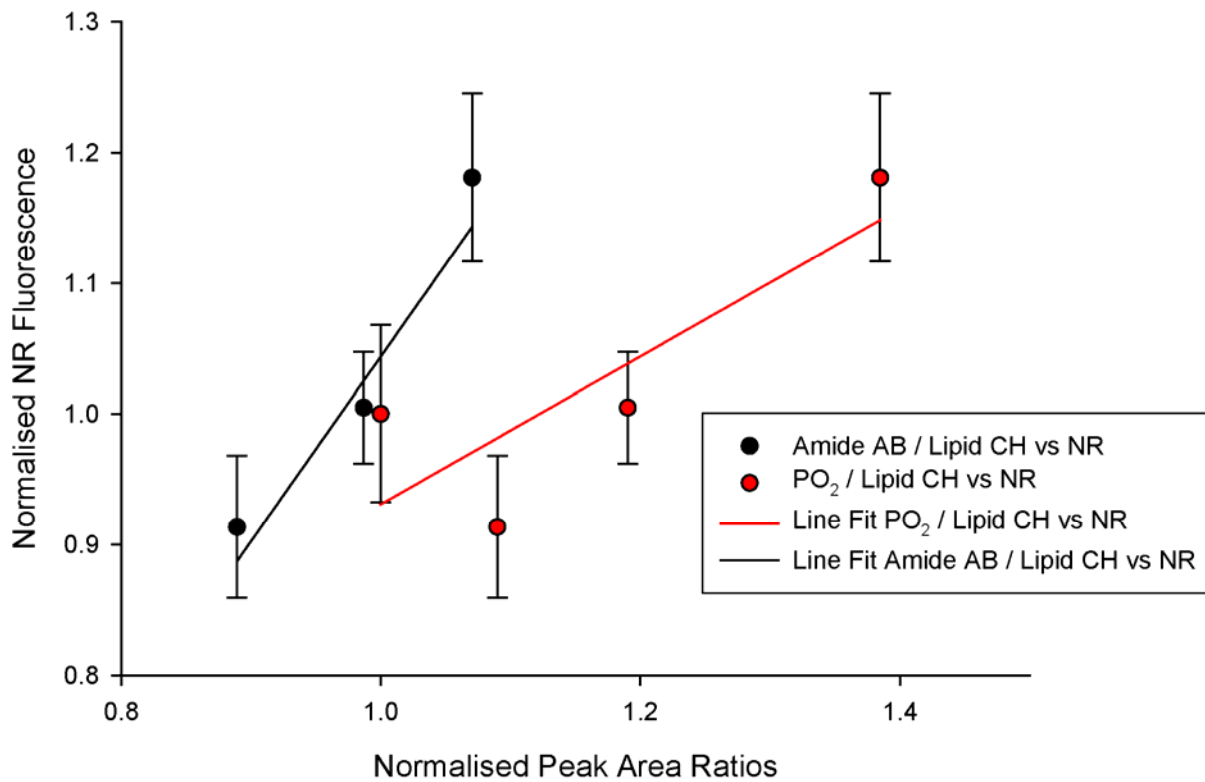
Figure 12. Correlation of various Raman band integrals (as described in the text) to NR fluorescence (cell viability) All measurements are normalised to the corresponding control measurement.
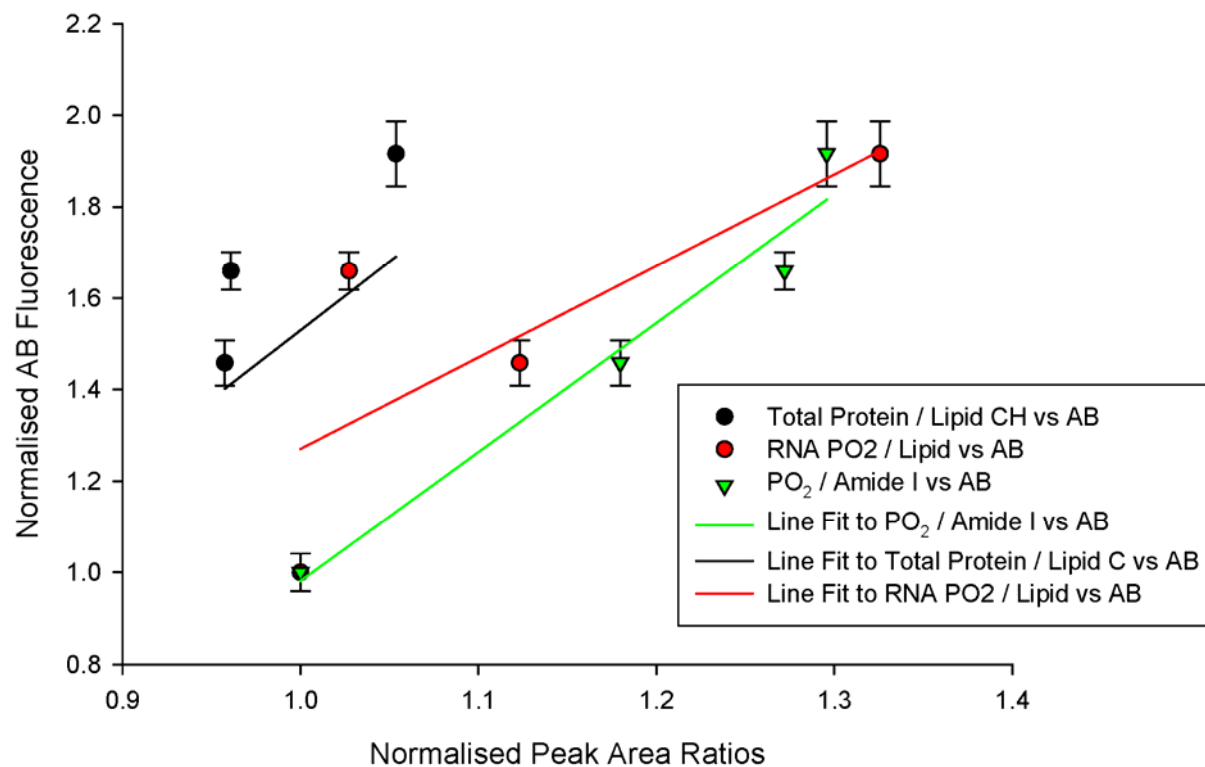

Figure 13. Correlation of various Raman band integrals (as described in the text) to AB fluorescence (proliferative capacity) All measurements are normalised to the corresponding control measurement.

Conclusion

Cell culture for spectroscopic measurements has not previously been performed with correction for the effects cell attachment has on cellular physiology. Recently it has been demonstrated in the literature that these effects can be expressed in the cell at the level of genomic regulation, thus contributing to very fundamental changes in cellular physiology, ultimately resulting in unknown adjustments to cellular proliferation, motility and, in some cases, phenotype [17-23]. In this work we have demonstrated that measurements of cellular proliferation and viability on coated spectroscopic substrates can be correlated with spectral changes induced by adjustments to cell physiology when cultured on the different coatings. These measurements demonstrate that the interaction of the cell with coated spectroscopic substrates can influence the spectroscopic measurement made using vibrational spectroscopy. Ultimately this implies that spectroscopic measurements made using Raman and IR spectroscopy, if they are to be used together to characterize cellular interaction with toxic agents, etc., should utilise a coating, such as gelatin, which harmonises the cell interaction with the spectroscopic substrate, such that the measurements are intercomparable and complementary. The measurements also demonstrate that vibrational spectroscopy can probe the results of cellular interactions occuring at genomic level, which can be significant to the development of these modalities in the future.

Acknowledgements

References

1. Gaudenzi S, Pozzi, D., Toro, P., Silvestri, I., Morrone, S., Castellano, C. Cell apoptosis specific marker found by Fourier Transform Infrared Spectroscopy. Spectroscopy 2004;18:415-422.
2. Notingher I, Selvakumaran J, Hench LL. New detection system for toxic agents based on continuous spectroscopic monitoring of living cells. Biosens Bioelectron 2004;20(4):780-9.
3. Uzunbajakava N, Lenferink A, Kraan Y, Volokhina E, Vrensen G, Greve J, et al. Nonresonant confocal Raman imaging of DNA and protein distribution in apoptotic cells. Biophys J 2003;84(6):3968-81.
4. Notingher I, Verrier S, Haque S, Polak JM, Hench LL. Spectroscopic study of human lung epithelial cells (A549) in culture: living cells versus dead cells. Biopolymers 2003;72(4):230-40.
5. Holman HYN, Martin, M.C., Blakely, E.A., Bjornstad, K., McKinney, W.R. IR spectroscopic characteristics of cell cycle and cell death probed by synchrotron radiation based fourier transform IR spectromicroscopy. Biopolymers (Biospectroscopy) 2000;57:329-335.
6. Short KW, Carpenter, S., Freyer, J. P., and Mourant, J. R. Raman Spectroscopy Detects Biochemical Changes Due to Proliferation in Mammalian Cell Cultures. Biophysical Journal 2005;88:4274-4288.
7. Mourant JR, Canpolat M, Brocker C, Esponda-Ramos O, Johnson TM, Matanock A, et al. Light scattering from cells: the contribution of the nucleus and the effects of proliferative status. J Biomed Opt 2000;5(2):131-7.
8. Mourant JR, Yamada YR, Carpenter S, Dominique LR, Freyer JP. FTIR spectroscopy demonstrates biochemical differences in mammalian cell cultures at different growth stages. Biophys J 2003;85(3):1938-47.
9. Matthaus C, Boydston-White S, Miljkovic M, Romeo M, Diem M. Raman and infrared microspectral imaging of mitotic cells. Appl Spectrosc 2006;60(1):1-8.
10. Notingher I, Bisson I, Bishop AE, Randle WL, Polak JM, Hench LL. In situ spectral monitoring of mRNA translation in embryonic stem cells during differentiation in vitro. Anal Chem 2004;76(11):3185-93.
11. Notingher I, Jell G, Lohbauer U, Salih V, Hench LL. In situ non-invasive spectral discrimination between bone cell phenotypes used in tissue engineering. J Cell Biochem 2004;92(6):1180-92.
12. Holman HYN, Bjornstad, K., Mc Namara, M.P., M.C. Martin, W.R. McKinney, E.A. Blakely. Synchrotron infrared spectromicroscopy as a novel bioanalytical microprobe for individual living cells: cytotoxicity considerations. J Biomed Opt 2002;7(3):417-424.
13. Notingher I, Verrier, S., Romanska, H., Bishop, A.E., Polak, J.M., Hench, L.L. In situ characterisation of living cells by Raman spectroscopy. Spectroscopy - Int. J. 2002;16(2):43-51.
14. Puppels GJ, Olminkhof JH, Segers-Nolten GM, Otto C, de Mul FF, Greve J. Laser irradiation and Raman spectroscopy of single living cells and chromosomes: sample degradation occurs with 514.5 nm but not with 660 nm laser light. Exp Cell Res 1991;195(2):361-7.
15. Ramser K, Bjerneld, E.J., Fant, C., Kall, M. Importance of substrate and photo-induced effects in Raman spectroscopy of single functional erythrocytes. Journal of Biomedical Optics 2003;8(2):173-178.
16. Keselowsky BG, Collard DM, Garcia AJ. Integrin binding specificity regulates biomaterial surface chemistry effects on cell differentiation. Proc Natl Acad Sci U S A 2005;102(17):5953-7.
17. Gaudet C, Marganski WA, Kim S, Brown CT, Gunderia V, Dembo M, et al. Influence of type I collagen surface density on fibroblast spreading, motility, and contractility. Biophys J 2003;85(5):3329-35.
18. Keselowsky BG, Collard DM, Garcia AJ. Surface chemistry modulates focal adhesion composition and signaling through changes in integrin binding. Biomaterials 2004;25(28):5947-54.
19. Garcia AJ, Vega MD, Boettiger D. Modulation of cell proliferation and differentiation through substrate-dependent changes in fibronectin conformation. Mol Biol Cell 1999;10(3):785-98.
20. Allen LT, Tosetto M, Miller IS, O'Connor DP, Penney SC, Lynch I, et al. Surface-induced changes in protein adsorption and implications for cellular phenotypic responses to surface interaction. Biomaterials 2006;27(16):3096-108.
21. Brodbeck WG, Shive MS, Colton E, Nakayama Y, Matsuda T, Anderson JM. Influence of biomaterial surface chemistry on the apoptosis of adherent cells. J Biomed Mater Res 2001;55(4):661-8.
22. Shen M, Horbett TA. The effects of surface chemistry and adsorbed proteins on monocyte/macrophage adhesion to chemically modified polystyrene surfaces. J Biomed Mater Res 2001;57(3):336-45.
23. Redey SA, Nardin M, Bernache-Assolant D, Rey C, Delannoy P, Sedel L, et al. Behavior of human osteoblastic cells on stoichiometric hydroxyapatite and type A carbonate apatite: role of surface energy. J Biomed Mater Res 2000;50(3):353-64.

24.	Boukamp P, Petrussevska RT, Breitkreutz D, Hornung J, Markham A, Fusenig NE. Normal keratinization in a spontaneously immortalized aneuploid human keratinocyte cell line. J Cell Biol 1988;106(3):761-71.

25.	Boudreau NJ, Jones, P.L. Extracellular matrix and integrin signalling : the shape of things to come. Biochem. J. 1999;339:481-488.

26.	Colognato H, Yurchenco PD. Form and function: the laminin family of heterotrimers. Dev Dyn 2000;218(2):213-34.

27.	Frushour BG, Koenig JL. Raman scattering of collagen, gelatin, and elastin. Biopolymers 1975;14(2):379-91.

28.	Mousia Z, Farhat IA, Pearson M, Chesters MA, Mitchell JR. FTIR microspectroscopy study of composition fluctuations in extruded amylopectin-gelatin blends. Biopolymers 2001;62(4):208-18.

29.	O'Brien J, Wilson, I., Orton T., Pognan, P. Investigation of the Alamar Blue (resazurin) fluorescent dye for the assessment of mammalian cell cytotoxicity. Eur. J. Biochem. 2000;267:5421-5426.

30.	Slaughter MR, Bugelski, P.J., O' Brien, P.J. Evaluation of Alamar Blue reduction for the in-vitro assay of hepatocyte toxicity. Toxicology In Vitro 1999;13:567-569.

31.	Borenfreund E, Puerner, J A. A simple quantitatve procedure using monolayer culture for cytotoxicity assays. J. Tissue Cult. Methods 1984;9:7-9.

32.	Mammone T, Gan D, Collins D, Lockshin RA, Marenus K, Maes D. Successful separation of apoptosis and necrosis pathways in HaCaT keratinocyte cells induced by UVB irradiation. Cell Biol Toxicol 2000;16(5):293-302.

33.	Zhang SZ, Lipsky MM, Trump BF, Hsu IC. Neutral red (NR) assay for cell viability and xenobiotic-induced cytotoxicity in primary cultures of human and rat hepatocytes. Cell Biol Toxicol 1990;6(2):219-34.

34.	Ahmad H, Saleemuddin M. A Coomassie blue-binding assay for the microquantitation of immobilized proteins. Anal Biochem 1985;148(2):533-41.

35.	Liebsch HM, Spielmann H. Balb/c 3T3 cytotoxicity test. Methods Mol Biol 1995;43:177-87.

36.	Ní Shúilleabháin S, Mothersill, C., Sheehan, D., O'Brien, N.M., O' Halloran, J., Van Pelt, F.N.A.M., Davoren M. In vitro cytotoxicity testing of three zinc metal salts using established fish cell lines. Toxicol In Vitro 2004;18(3):365-376.

37.	Murali Krishna C, Kegelaer G, Adt I, Rubin S, Kartha VB, Manfait M, et al. Characterisation of uterine sarcoma cell lines exhibiting MDR phenotype by vibrational spectroscopy. Biochim Biophys Acta 2005;1726(2):160-7.

38.	Nijssen A, Bakker Schut TC, Heule F, Caspers PJ, Hayes DP, Neumann MH, et al. Discriminating basal cell carcinoma from its surrounding tissue by Raman spectroscopy. J Invest Dermatol 2002;119(1):64-9.

39.	Synytsya A, Alexa P, Besserer J, De Boer J, Froschauer S, Gerlach R, et al. Raman spectroscopy of tissue samples irradiated by protons. Int J Radiat Biol 2004;80(8):581-91.

40.	Edwards HGM, Carter, E.A. Biological Applications of Raman Spectroscopy. Infrared and Raman Spectroscopy of Biological Materials (Practical Spectroscopy) 2000;Gremlich, H.U., and Yan, B. eds:421-477.

41.	Puppels GJ, Garritsen HS, Segers-Nolten GM, de Mul FF, Greve J. Raman microspectroscopic approach to the study of human granulocytes. Biophys J 1991;60(5):1046-56.

42.	Gault N, Lefaix JL. Infrared microspectroscopic characteristics of radiation-induced apoptosis in human lymphocytes. Radiat Res 2003;160(2):238-50.

43.	Gault N, Poncy JL, Lefaix JL. [Radiation-induced apoptosis: a new approach using infrared microspectroscopy]. Can J Physiol Pharmacol 2004;82(1):38-49.

44.	Gault N, Rigaud O, Poncy JL, Lefaix JL. Infrared microspectroscopy study of gamma-irradiated and H(2)O(2)-treated human cells. Int J Radiat Biol 2005;81(10):767-779.

45.	Zellmer S, Zimmermann I, Selle C, Sternberg B, Pohle W, Lasch J. Physicochemical characterisation of human stratum corneum lipid liposomes. Chem Phys Lipids 1998;94(1):97-108.

46.	Evis Z, Sato M, Webster TJ. Increased osteoblast adhesion on nanograined hydroxyapatite and partially stabilized zirconia composites. J Biomed Mater Res A 2006.

47.	Rouahi M, Gallet O, Champion E, Dentzer J, Hardouin P, Anselme K. Influence of hydroxyapatite microstructure on human bone cell response. J Biomed Mater Res A 2006.

48.	Zhu X, Eibl O, Scheideler L, Geis-Gerstorfer J. Characterization of nano hydroxyapatite/collagen surfaces and cellular behaviors. J Biomed Mater Res A 2006.

49.	Chun J, Auer KA, Jacobson BS. Arachidonate initiated protein kinase C activation regulates HeLa cell spreading on a gelatin substrate by inducing F-actin formation and exocytotic upregulation of beta 1 integrin. J Cell Physiol 1997;173(3):361-70.

50.	Bill HM, Knudsen B, Moores SL, Muthuswamy SK, Rao VR, Brugge JS, et al. Epidermal growth factor receptor-dependent regulation of integrin-mediated signaling and cell cycle entry in epithelial cells. Mol Cell Biol 2004;24(19):8586-99.

51.	Putnins EE, Firth JD, Lohachitranont A, Uitto VJ, Larjava H. Keratinocyte growth factor (KGF) promotes keratinocyte cell attachment and migration on collagen and fibronectin. Cell Adhes Commun 1999;7(3):211-21.

52.   Doornaert B, Leblond V, Planus E, Galiacy S, Laurent VM, Gras G, et al. Time course of actin cytoskeleton stiffness and matrix adhesion molecules in human bronchial epithelial cell cultures. Exp Cell Res 2003;287(2):199-208.

53.   Sutherland J, Denyer M, Britland S. Motogenic substrata and chemokinetic growth factors for human skin cells. J Anat 2005;207(1):67-78.

54.   Brumfeld V, Werber MM. Studies on fibronectin and its domains. II. Secondary structure and spatial configuration of fibronectin and of its domains. Arch Biochem Biophys 1993;302(1):134-43.

55.   Gazi E, Dwyer, J., Lockyer, N.P., Miyan, J., Gardner, P., Hart, C., Brown, M., Clarke, N. W. Fixation Protocols for Subcellular Imaging by Synchrotron-Based Fourier Transform Infrared Microspectroscopy. Biopolymers 2005;77:18-30.

56.   O Faolain E, Hunter MB, Byrne JM, Kelehan P, McNamara M, Byrne HJ, et al. A study examining the effects of tissue processing on human tissue sections using vibrational spectroscopy. Vibrational Spectroscopy 2005;38(1-2):121-127.

57.   Krishna CM, Sockalingum GD, Kurien J, Rao L, Venteo L, Pluot M, et al. Micro-Raman spectroscopy for optical pathology of oral squamous cell carcinoma. Appl Spectrosc 2004;58(9):1128-35.